PERGAMON

International Journal of Solids and Structures 38 (2001) 7447–7460

INTERNATIONAL JOURNAL OF SOLIDS and STRUCTURES

www.elsevier.com/locate/ijsolstr

Taylor-based nonlocal theory of plasticity: numerical studies of the micro-indentation experiments and crack tip fields

Y. Guo [a], Y. Huang [b,*], H. Gao [c], Z. Zhuang [a], K.C. Hwang [a]

[a] *Failure Mechanics Laboratory, Department of Engineering Mechanics, Tsinghua University, Beijing 100084, People's Republic of China*
[b] *Department of Mechanical and Industrial Engineering, University of Illinois, 1206 W. Green Street, Urbana, IL 61801, USA*
[c] *Division of Mechanics and Computation, Stanford University, Palo Alto, CA 94305, USA*

Received 19 July 2000

Abstract

Recent advances in strain gradient plasticity have provided a means to quantitatively characterize the experimentally observed size effect at the micron and submicron scales. The introduction of strain gradients in the constitutive model has increased the order of governing equations and therefore require additional boundary conditions in some theories of strain gradient plasticity. Is it possible to develop a micro-scale plasticity theory that preserves the structure of classical plasticity? The Taylor-based nonlocal theory (TNT) of plasticity (Int. J. Solids Struct. 38 (2001), 2615) was developed from the Taylor dislocation model for this purpose. We have proposed a finite element method for TNT plasticity, and have applied it to study micro-indentation experiments. The micro-indentation hardness predicted by TNT plasticity agrees very well with the indentation hardness data. We have also studied the crack tip field in TNT plasticity, and have found that the stress level in TNT plasticity is significantly higher than that in classical plasticity. This provides an alternative mechanism for cleavage fracture in ductile materials observed in Elssner et al.'s experiments (Scripta Metall. Mater. 31 (1994) 1037).

Keywords: Taylor model; Nonlocal plasticity; Crack tip fields; Micro-indentation

1. Introduction

Classical theories of plasticity fail to explain the size-dependent material behavior repeatedly observed in micro-indentation hardness experiments (Nix, 1989, 1997; De Guzman et al., 1993; Stelmashenko et al., 1993; Atkinson, 1995; Ma and Clarke, 1995; Poole et al., 1996; McElhaney et al., 1998; Suresh et al., 2000) as well as in micro-torsion (Fleck et al., 1994), micro-bend experiments (Stolken and Evans, 1998) and metal–matrix composites (Lloyd, 1994). These experiments have shown "the smaller, the harder" material behavior at the micron and submicron scales. This size-dependent material behavior has also been confirmed by the direct simulations of dislocation interaction and motion (Cleveringa et al., 1997, 1998,

* Corresponding author. Tel.: +1-217-265-5072; fax: +1-217-244-6534.
E-mail address: huang9@uiuc.edu (Y. Huang).

0020-7683/01/$ - see front matter
PII: S0020-7683(01)00047-6

1999a,b, 2000; Needleman, 2000). Based on the notion of geometrically necessary dislocations in dislocation mechanics (Ashby, 1970; Arsenlis and Parks, 1999; Gurtin, 2000), theories of strain gradient plasticity have been developed to model materials and structures whose dimension controlling plastic deformation falls roughly within a range from 0.1 to 10 μm. Some strain gradient theories involve higher-order stresses such that the order of governing equations increases and additional boundary conditions are needed (e.g., Fleck and Hutchinson, 1993, 1997; Fleck et al., 1994; Gao et al., 1999a,b; Huang et al., 1999, 2000a,b; Shu and Fleck, 1999). Is it possible to develop a continuum plasticity theory that captures the size-dependent material behavior at the micron scale, but preserves the structure of classical continuum theories? Acharya and Bassani (2000), Acharya and Beaudoin (2000), Beaudoin et al. (2000) and Dai and Parks (2001) introduced strain gradients in the incremental stress–strain relation through the plastic work hardening moduli. Phenomenological expressions of the hardening moduli were assumed and the length parameter scaling the strain gradients were determined by fitting experiments at the micron scale. From a different approach, Gao and Huang (2001) developed the Taylor-based nonlocal theory (TNT) of plasticity from the Taylor model in dislocation mechanics. It falls into the framework of nonlocal plasticity theories (e.g., Eringen, 1981, 1983; Bazant et al., 1984; Bazant, 1986; Pijaudier-Cabot and Bazant, 1987; Bazant and Lin, 1988; Stromberg and Ristinmaa, 1996; Chen, 1999) such that the basic balance laws are identical to the classical theories. It does not involve higher-order stresses nor additional boundary conditions, and the order of governing equations remains the same as that of classical plasticity. Gao and Huang (2001) showed that TNT plasticity agrees well with the micro-bend (Stolken and Evans, 1998) and micro-torsion experiments (Fleck et al., 1994).

In this paper, we develop the finite element method for TNT plasticity. We use the numerical method to investigate an important class of micro-scale experiments, namely the micro-indentation hardness tests, and compare the numerically predicted micro-indentation hardness with the experimental hardness data. We then present a numerical study of the crack tip field in TNT plasticity, which has direct implications on the experimentally observed cleavage fracture in ductile materials (Elssner et al., 1994).

2. Taylor-based nonlocal theory of plasticity

The balance law in TNT plasticity is identical to that of the classical theories (e.g., Eringen, 1981, 1983),

$$\sigma_{ij,i} + f_j = 0, \tag{1}$$

where f_j denotes the body force, and σ_{ij} is the symmetric stress tensor. Before we present the deformation and flow theories of TNT plasticity, we first discuss the flow stress established from the Taylor dislocation model.

2.1. Flow stress and nonlocal integral representation of strain gradient

The Taylor dislocation model gives the shear flow stress τ in terms of the dislocation density ρ as $\tau = \alpha\mu b\sqrt{\rho}$, where μ is the shear modulus, b is the Burgers vector, and α is an empirical coefficient between 0.1 and 1 (Nix and Gibeling, 1985). The dislocation density ρ is composed of the density of statistically stored dislocations, ρ_S, and that of geometrically necessary dislocations, ρ_G. It is well known that ρ_G is linearly proportional to the local curvature of deformation, i.e., strain gradient (Ashby, 1970; Nix and Gao, 1998), while ρ_S is related to the uniaxial stress–strain curve (Nix and Gao, 1998). Based on the above considerations, Nix and Gao (1998), Gao et al. (1999b), and Huang et al. (2000b) established the flow stress accounting for the effect of geometrically necessary dislocations as

$$\sigma = \sigma_{\text{ref}}\sqrt{f^2(\epsilon) + \ell\eta}, \tag{2}$$

where $\sigma = \sigma_{\text{ref}} f(\epsilon)$ is the uniaxial stress–strain relation, σ_{ref} is a reference stress in uniaxial tension, η is the effective strain gradient to be discussed later, and the internal material length ℓ scaling the strain gradient is given in terms of the shear modulus μ, Burgers vector b and the coefficient α in the Taylor model by

$$\ell = 18\alpha^2 \left(\frac{\mu}{\sigma_{\text{ref}}} \right)^2 b. \tag{3}$$

It should be pointed out that the flow stress in Eq. (2) is independent of σ_{ref}. This becomes clear when we rewrite Eq. (2) as

$$\sigma = \sqrt{[\sigma_{\text{ref}} f(\epsilon)]^2 + 18\alpha^2 \mu^2 b \eta},$$

which depends on the uniaxial stress–strain relation $\sigma_{\text{ref}} f(\epsilon)$ but not on the choice of σ_{ref}. Only when we want to define the internal material length ℓ in Eq. (3) the reference stress σ_{ref} is needed.

The effective strain gradient η in Eq. (2) is related to the density of geometrically dislocations ρ_{G} by $2\eta = \rho_{\text{G}} b$, where the factor of 2 is the so-called Nye factor (Arsenlis and Parks, 1999; Huang et al., 2000b) for a polycrystalline material. Based on models of geometrically necessary dislocations for pure bending, pure torsion and void growth, Gao et al. (1999b) determined η in terms of the deviatoric strain gradient tensor η'_{ijk} as

$$\eta = \sqrt{\tfrac{1}{4}\eta'_{ijk}\eta'_{ijk}}, \tag{4}$$

where

$$\eta'_{ijk} = \epsilon_{ik,j} + \epsilon_{jk,i} - \epsilon_{ij,k} - \tfrac{1}{4}\left(\delta_{ik}\epsilon_{pp,j} + \delta_{jk}\epsilon_{pp,i}\right), \tag{5}$$

is obtained from the spatial gradient of strains. Accordingly, the order of governing equations increases, and additional boundary conditions are needed in strain gradient plasticity (e.g., Fleck and Hutchinson, 1997; Gao et al., 1999b; Huang et al., 1999, 2000a,b).

In TNT plasticity, the strain gradient tensor is evaluated via the nonlocal integral of strains such that the essential structure of classical plasticity theory is preserved and no additional boundary conditions are needed. Let $\boldsymbol{x}$ denote a material point in the solid, and $\boldsymbol{\xi}$ be the local Cartesian coordinate origined at $\boldsymbol{x}$. The strain in the vicinity of $\boldsymbol{x}$ can be expanded in Taylor series as

$$\epsilon_{ij}(\boldsymbol{x} + \boldsymbol{\xi}) = \epsilon_{ij}(\boldsymbol{x}) + \epsilon_{ij,k}(\boldsymbol{x})\xi_k + \mathrm{O}(|\boldsymbol{\xi}|^2). \tag{6}$$

As in any nonlocal continuum theories, each material point $\boldsymbol{x}$ is surrounded by a mesoscale cell, V_{cell}. The cell size and its effect on the numerical results are discussed in detail in Section 3. Multiplying ξ_m on both sides of Eq. (6) and integrating over the mesoscale cell gives the nonlocal integral representation of the strain gradient tensor as

$$\epsilon_{ij,k} = \int_{V_{\text{cell}}} \left[\epsilon_{ij}(\boldsymbol{x} + \boldsymbol{\xi}) - \epsilon_{ij}(\boldsymbol{x})\right] \xi_m \, \mathrm{d}V \left(\int_{V_{\text{cell}}} \xi_m \xi_k \, \mathrm{d}V \right)^{-1}, \tag{7}$$

where $\left(\int_{V_{\text{cell}}} \xi_m \xi_k \, \mathrm{d}V \right)^{-1}$ is the inverse of matrix $\int_{V_{\text{cell}}} \xi_m \xi_k \, \mathrm{d}V$. The deviatoric strain gradient tensor η'_{ijk} in Eq. (5) is then readily expressed in terms of the nonlocal integrals of strains via Eq. (7). This representation of the strain gradient tensor does not increase the order of governing equations, and therefore does not require additional boundary conditions.

2.2. Deformation theory of TNT plasticity

The strains are decomposed into a volumetric part and a deviatoric part,

$$\epsilon_{ij} = \tfrac{1}{3}\epsilon_{kk}\delta_{ij} + \epsilon'_{ij}. \tag{8}$$

The volumetric strain is related to the hydrostatic stress σ_{kk} via the elastic bulk modulus K,

$$\epsilon_{kk} = \frac{\sigma_{kk}}{3K}. \tag{9}$$

The deviatoric strains are proportional to deviatoric stresses $\sigma'_{ij} = \sigma_{ij} - \frac{1}{3}\sigma_{kk}\delta_{ij}$ such that

$$\epsilon'_{ij} = \frac{3\epsilon}{2\sigma_{\mathrm{e}}}\sigma'_{ij}, \tag{10}$$

where $\epsilon = \sqrt{\frac{2}{3}\epsilon'_{ij}\epsilon'_{ij}}$ and $\sigma_{\mathrm{e}} = \sqrt{\frac{3}{2}\sigma'_{ij}\sigma'_{ij}}$ are the effective strain and effective stress, respectively.

The yield criterion is

$$\sigma_{\mathrm{e}} = \sigma, \tag{11}$$

where the flow stress is given in Eq. (2). Combining the above relations leads to the following constitutive equations for the deformation theory of TNT plasticity:

$$\sigma_{kk} = 3K\epsilon_{kk}, \qquad \sigma'_{ij} = \frac{2\sigma_{\mathrm{ref}}\sqrt{f^2(\epsilon) + \ell\eta}}{3\epsilon}\epsilon'_{ij}, \tag{12}$$

where the effective strain gradient η is given in terms of the nonlocal integrals of strains via Eqs. (4), (5) and (7).

2.3. Flow theory of TNT plasticity

The strain rates are decomposed into the elastic and plastic parts as

$$\dot{\epsilon}_{ij} = \dot{\epsilon}^{\mathrm{e}}_{ij} + \dot{\epsilon}^{\mathrm{p}}_{ij} = \frac{\dot{\sigma}_{kk}}{9K}\delta_{ij} + \frac{\dot{\sigma}'_{ij}}{2\mu} + \dot{\epsilon}^{\mathrm{p}}_{ij}, \tag{13}$$

where the elastic strain rates are related to the stress rates through the elastic shear and bulk moduli, μ and K, respectively; and the plastic strain rates are proportional to the deviatoric stress σ'_{ij},

$$\dot{\epsilon}^{\mathrm{p}}_{ij} = \frac{3\dot{\epsilon}^{\mathrm{p}}}{2\sigma_{\mathrm{e}}}\sigma'_{ij} \quad \text{if } \dot{\epsilon}^{\mathrm{p}} > 0, \tag{14}$$

where $\dot{\epsilon}^{\mathrm{p}} = \sqrt{\frac{2}{3}\dot{\epsilon}^{\mathrm{p}}_{ij}\dot{\epsilon}^{\mathrm{p}}_{ij}}$ and $\sigma_{\mathrm{e}} = \sqrt{\frac{3}{2}\sigma'_{ij}\sigma'_{ij}}$ are the effective plastic strain rate and effective stress, respectively. The nondecreasing accumulative plastic strain ϵ^{p} is obtained from the effective plastic strain rate by

$$\epsilon^{\mathrm{p}} = \int_0^t \dot{\epsilon}^{\mathrm{p}}\,\mathrm{d}t. \tag{15}$$

The yield criterion is the same as that in Eq. (11), but the flow stress in Eq. (2) is rewritten in terms of the plastic strain in Eq. (15) and the effective strain gradient in Eq. (4) as

$$\sigma = \sigma_{\mathrm{ref}}\sqrt{f^2_{\mathrm{p}}(\epsilon^{\mathrm{p}}) + \ell\eta}, \tag{16}$$

where the internal material length is given in Eq. (3), the uniaxial stress–strain relation is expressed in terms of the plastic strain ϵ^{p} as $\sigma = \sigma_{\mathrm{ref}} f_{\mathrm{p}}(\epsilon^{\mathrm{p}})$, and the function f_{p} is determined implicitly by

$$f_{\mathrm{p}}(\epsilon^{\mathrm{p}}) = f(\epsilon) = f\left[\epsilon^{\mathrm{p}} + \frac{\sigma_{\mathrm{ref}}}{E}f_{\mathrm{p}}(\epsilon^{\mathrm{p}})\right]. \tag{17}$$

The consistency condition is obtained from the incremental form of the yield condition (11) and flow stress in Eq. (16),

$$2\sigma_e\dot{\sigma}_e = 3\sigma'_{ij}\dot{\sigma}'_{ij} = \sigma^2_{ref}[2f_p f'_p\dot{\epsilon}^p + \ell\dot{\eta}], \tag{18}$$

where

$$\dot{\eta} = \frac{1}{4\eta}\eta'_{ijk}\dot{\eta}'_{ijk}. \tag{19}$$

Combining these relations and accounting for the effect of elastic unloading lead to the following constitutive equations for the flow theory of TNT plasticity,

$$\dot{\sigma}_{kk} = 3K\dot{\epsilon}_{kk}, \quad \dot{\sigma}'_{ij} = 2\mu\left(\dot{\epsilon}'_{ij} - \frac{3\sigma'_{ij}}{2\sigma}\dot{\epsilon}^p\right), \tag{20}$$

where $\dot{\epsilon}'_{ij} = \dot{\epsilon}_{ij} - \frac{1}{3}\dot{\epsilon}_{kk}\delta_{ij}$ is the deviatoric strain rate tensor, σ is the flow stress in Eq. (16), and the effective plastic strain rate is given by

$$\begin{aligned} \dot{\epsilon}^p &= \frac{6\mu\sigma'_{ij}\dot{\epsilon}'_{ij} - \sigma^2_{ref}\ell\dot{\eta}}{6\mu\sigma_e + 2\sigma^2_{ref}f_p f'_p} \quad \text{if } \sigma_e = \sigma \text{ and } 6\mu\sigma'_{ij}\dot{\epsilon}'_{ij} - \sigma^2_{ref}\ell\dot{\eta} \geqslant 0, \\ &= 0 \qquad\qquad\qquad\quad \text{if } \sigma_e < \sigma \text{ or } 6\mu\sigma'_{ij}\dot{\epsilon}'_{ij} - \sigma^2_{ref}\ell\dot{\eta} < 0. \end{aligned} \tag{21}$$

3. Finite element method for TNT plasticity

The finite element method for TNT plasticity is based on the principle of virtual work,

$$\int_V \boldsymbol{\sigma}\cdot\delta\boldsymbol{\epsilon}\,\mathrm{d}V = \int_S \boldsymbol{T}\cdot\delta\boldsymbol{u}\,\mathrm{d}S, \tag{22}$$

where the body force is neglected, and the integration is over the volume V and surface S of the solid. For a two-dimensional problem (e.g., plane–strain or axisymmetric analyses), we have used the nine-node element in the finite element analysis (Fig. 1). The isoparametric transform is used such that each element is transformed to a square (Fig. 1) in the isoparametric space. Strains, strain gradients and stresses are

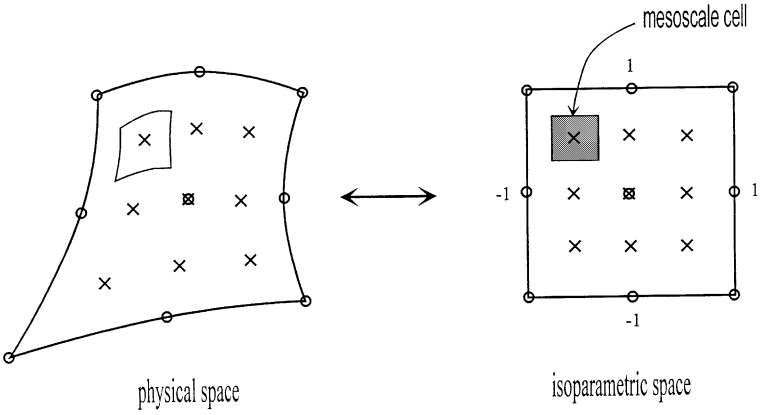

Fig. 1. A schematic diagram of the isoparametric transform. The mesoscale cell is taken as a little cubic (square) surrounding each Gaussian integration point in the isoparametric space.

evaluated at the Gaussian integration points in each element. The displacement field is interpolated by the element shape functions and the nodal displacements. The strain field can then be obtained from the strain–displacement relation. Since Eq. (22) is identical to that in the classical continuum theory, we discuss in the following only features that are unique in TNT plasticity.

For a two-dimensional problem, it can be shown that the three-dimensional integration in the mesoscale cell naturally degenerates to the two-dimensional integration. As shown in Fig. 1, we have taken the mesoscale cell to be a square (for a two-dimensional problem) surrounding the Gaussian integration points in the isoparametric space. The size of the mesoscale cell in the isoparametric space must be small such that it is completely contained in the element. Specifically, for an element size of 2 in the isoparametric space, the mesoscale cell size must be less than 0.45 for the element with nine-point Gaussian integration (see Fig. 1). In fact, we have taken a wide range of the mesoscale cell size in the present study, 0.4, 0.2, 0.02 and 0.002, and have found that the differences in numerical results never exceed 0.1%. In the following, we have taken the mesoscale cell size to be 0.002 in the isoparametric space.

It should be pointed out that there are two different levels of Gaussian integration in the finite element analysis for TNT plasticity. The first is at the element level, which is the same as classical plasticity theories. Stresses and strains are evaluated at the Gaussian integration points in each element. The second is at the mesoscale cell level, which is special for TNT plasticity. There is a mesoscale cell surrounding each element-level Gaussian integration point. Strains in the element (including the mesoscale cell) are interpolated by the nodal displacements. Accordingly, the nonlocal integral terms are also expressed in terms of the nodal displacements via Gaussian integration in the mesoscale cell.

It is important to account for the contribution from nonlocal terms to the overall stiffness matrix in the finite element method for TNT plasticity. In classical plasticity, stress increments in the element can be expressed in terms of the strain increments at the same Gaussian integration point via the incremental moduli. In TNT plasticity, however, stress increments depend not only on the strain increments at the same Gaussian integration point, but also on the nonlocal integration of strain increments in the mesoscale cell. Fortunately, the nonlocal integral terms in the element are expressed in terms of nodal displacements such that the principle of virtual work can still be recast into governing equations for the nodal displacements, though the stiffness matrix is not necessary symmetric anymore.

In order to validate the proposed numerical approach, we have compared the numerical results with analytic solutions for pure bending and axisymmetric growth of micro-voids (Gao and Huang, 2001). The numerical solutions agree very well with the analytic solutions. In the following, we use the finite element method for TNT plasticity to investigate a few phenomena that are important at the micron and submicron scales.

4. Numerical studies of micro-indentation experiments

Micro-indentation experiments provide a robust and reliable method to measure the mechanical properties of materials at the small scale. Strain gradient plasticity theories have been used to study the depth dependence of indentation hardness (Begley and Hutchinson, 1998; Shu and Fleck, 1998; Huang et al., 2000b). In this section we use the same indentation model of Begley and Hutchinson (1998) and Huang et al. (2000b) to simulate micro-indentation experiments with the deformation and flow theories of TNT plasticity. Accordingly, the model is only briefly summarized in this section. Readers are referred to the above papers for details.

We simulate a frictionless, axisymmetric conical indenter, with the half of cone angle being 72°, corresponding to a Vickers indenter. Following Begley and Hutchinson (1998) and Huang et al. (2000b), the normal displacement is prescribed over the contact area of indentation. For a given depth of indentation, the radius of contact is determined by requiring the normal stress to vanish at the periphery of contact. The

hardness H is defined by the average contact pressure, i.e., the ratio of indentation load to the actual contact area. When the depth of indentation becomes much larger than the internal material length ℓ in Eq. (3), strain gradient effects disappear and the corresponding hardness does not display any depth dependence. This hardness, denoted by H_0 in order to distinguish from H, is the hardness in classical plasticity.

The material properties are taken from the micro-indentation experiments of McElhaney et al. (1998) for a polycrystalline copper: Burgers vector $b = 0.255$ nm, elastic shear modulus $\mu = 42$ GPa, Poisson's ratio $\nu = 0.3$, plastic work hardening exponent $N = 0.3$, the uniaxial stress–strain relation $\sigma = 688\epsilon^{0.3}$ MPa, which gives $H_0 = 834$ MPa for large depths of indentation (without strain gradient effects), consistent with that reported in the experiments of McElhaney et al. (1998).

The depth dependence of micro-indentation hardness predicted by TNT plasticity is shown in Fig. 2. The square of micro-indentation hardness, H^2, normalized by H_0^2 is plotted versus the inverse of the depth of indentation, $1/h$, as suggested by Nix and Gao (1998). Both the deformation and flow theories of TNT plasticity and the experimental data of McElhaney et al. (1998) are presented in Fig. 2. The empirical coefficient in the Taylor model is $\alpha = 0.30$, which indeed has the correct order of magnitude. It is observed that the difference between the deformation and flow theories of TNT plasticity is rather small, and both agree very well with the experimental data over a wide range of indentation depth, from one-tenth of a micron to several microns. This indicates that TNT plasticity can characterize the plastic behavior of materials rather accurately at the micron and submicrons scales.

Both TNT plasticity (Gao and Huang, 2001) and the mechanism-based strain gradient (MSG) plasticity theory (Gao et al., 1999b; Huang et al., 1999, 2000a,b) are based on the Taylor dislocation model, but they belong to different theoretical frameworks; MSG plasticity is a local plasticity theory involving higher-order stresses, while TNT plasticity is a nonlocal plasticity theory without higher-order stresses. Qiu et al. (2001) used the MSG plasticity theory to study the micro-indentation experiments. The additional boundary condition imposed was the vanishing of higher-order stress traction. For the same material parameters as in this section, MSG and TNT plasticity give identical micro-indentation hardness. This verifies the conclusion established in the prior study that MSG and TNT plasticity give essentially the same results if the

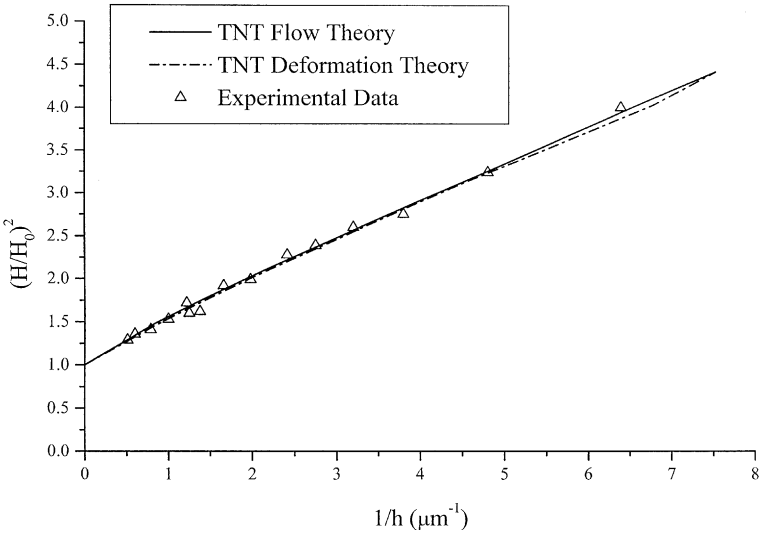

Fig. 2. The square of micro-indentation hardness, H^2, versus the inverse of indentation depth, $1/h$, predicted by the flow and deformation theories of TNT plasticity and the experimental data of McElhaney et al. (1998); the shear modulus $\mu = 42$ GPa, Poisson's ratio $\nu = 0.3$, and the uniaxial stress–strain relation $\sigma = 688\epsilon^{0.3}$ MPa, which gives the indentation hardness $H_0 = 834$ MPa for large depths of indentation; Burgers vector $b = 0.255$ μm, and Taylor coefficient $\alpha = 0.30$.

higher-order stress traction vanishes on the boundary (Gao and Huang, 2001). However, MSG plasticity theory gives a boundary-layer solution if the higher-order stress traction does not vanish on the boundary (Gao et al., 1999b). Solutions predicted by MSG and TNT plasticity are certainly different within the boundary layer. Such boundary layers have also been observed in the direct dislocation simulations (Shu et al., 2001).

5. Crack tip fields in TNT plasticity

5.1. Motivation of the present work

In a remarkable series of experiments, Elssner et al. (1994) measured both the macroscopic fracture toughness and atomic work of separation of an interface between a single crystal of niobium and a sapphire single crystal. The macroscopic work of fracture was two to three orders of magnitude higher than the atomic work of separation. This large difference was attributed to significant plastic dissipation in niobium. According to models based on the classical theories of plasticity, the maximum stress level that can be achieved near a crack tip is no more than four to five times the yield stress of the material (Hutchinson, 1997). However, Elssner et al. (1994) observed that interface between niobium and sapphire remained atomistically sharp. The stress level needed to produce atomic decohesion of a lattice or a strong interface is typically 0.03 times the Young's modulus, or equivalently 10 times the yield stress (Hutchinson, 1997), which is more than twice the maximum stress level predicted by classical plasticity. The classical plasticity theories clearly fall short of reaching the stress level to trigger cleavage fracture in presence of plastic flow observed in the experiments of Elssner et al. (1994).

Several models have been developed to identify potential mechanisms for cleavage fracture in ductile materials (e.g., Suo et al., 1993; Beltz et al., 1996; Wei and Hutchinson, 1999). In this section, we provide an alternative approach based on TNT plasticity. We use the finite element method in Section 3 to study fracture in TNT plasticity. The strain gradient effects associated with geometrically necessary dislocations significantly increase the stress level near a crack tip, and therefore provide an alternative mechanism for cleavage fracture in presence of plastic flow observed in the experiments of Elssner et al. (1994).

5.2. Model of fracture in TNT plasticity

We study plane–strain, mode-I fracture in TNT plasticity. We have taken a circular domain of radius $10^3\ell$ centered at the crack tip, where ℓ is the internal material length in TNT plasticity given in Eq. (3). The mode-I elastic K field is imposed on the outer boundary of the circular domain (polar radius $r = 10^3\ell$). This model provides a clear picture of the transition from the remote elastic K field to the near-tip field in TNT plasticity. The crack faces (polar angles $\theta = \pm\pi$) remain fraction free.

Only the upper half plane is analyzed due to symmetry. A very fine mesh is used near the crack tip, with the smallest element size less than $10^{-3}\ell$. Mesh refinement has ensured that the numerical results are accurate. The mesoscale cell size has been fixed at 0.002 in the isoparametric space (Fig. 1), though we have taken other values (as large as 0.4) and the finite element results are essentially independent of the mesoscale cell size.

We have used the following piecewise elastic–plastic stress–strain relation in uniaxial tension in order to clearly define plastic yielding,

$$\begin{aligned} \sigma = \sigma_{\mathrm{ref}} f(\epsilon) &= E\epsilon \qquad \epsilon < \frac{\sigma_{\mathrm{Y}}}{E}, \\ &= \sigma_{\mathrm{ref}}\epsilon^N \quad \epsilon \geqslant \frac{\sigma_{\mathrm{Y}}}{E}, \end{aligned} \tag{23}$$

where E is the elastic modulus, σ_Y the yield stress, N the plastic work hardening exponent ($0 \leqslant N < 1$), and the reference stress $\sigma_{ref} = \sigma_Y(E/\sigma_Y)^N$. The above equation can be rearranged to give an implicit relation $\sigma = \sigma_{ref} f_p(\epsilon^p)$ between stress and plastic strain in uniaxial tension as

$$\sigma = \sigma_{ref}\left[\frac{\sigma}{E} + \epsilon^p\right]^N \quad \sigma \geqslant \sigma_Y. \tag{24}$$

5.3. Normalization

The stresses σ_{ij} and displacements u_i are normalized by the yield stress σ_Y and the internal material length ℓ in TNT plasticity given in Eq. (3), respectively,

$$\frac{\sigma_{ij}}{\sigma_Y} = \sigma_{ij}^0\left(\frac{r}{l}, \theta, N = 0.2, \frac{\sigma_Y}{E} = 0.2\%, v = 0.3, \frac{K_I}{\sigma_Y l^{1/2}}\right), \tag{25}$$

$$\frac{u_i}{\ell} = u_i^0\left(\frac{r}{l}, \theta, N = 0.2, \frac{\sigma_Y}{E} = 0.2\%, v = 0.3, \frac{K_I}{\sigma_Y l^{1/2}}\right), \tag{26}$$

where σ_{ij}^0 and u_i^0 are nondimensional functions of the distance r to the crack tip (normalized by ℓ), polar angle θ; unless otherwise specified, the plastic work hardening exponent $N = 0.2$, the ratio of yield stress to Young's modulus $\sigma_Y/E = 0.2\%$, and the Poisson's ratio $v = 0.3$ in the following; K_I is the remote stress intensity factor of the elastic K field imposed on the outer boundary of the finite element domain. The normalized stresses and displacements do not depend explicitly on the Taylor coefficient α since α has been absorbed into the internal material length ℓ in Eq. (3).

5.4. Numerical results

Fig. 3 shows the normalized effective stress, σ_e/σ_Y, versus the normalized distance ahead of the crack tip, r/l, for both the flow and deformation theories of TNT plasticity. The polar angle $\theta = 1.014°$, and the remote stress intensity factor is $K_I/\sigma_Y\ell^{1/2} = 20$. The corresponding curve for the classical flow theory of plasticity (without strain gradient effects) is also shown in Fig. 3. The horizontal line $\sigma_e/\sigma_Y = 1$ separates the elastic and plastic zones for each curve. It is observed that the flow and deformation theories of TNT plasticity give the same stress distribution over the entire range of r. The curves for TNT plasticity and classical plasticity can be roughly divided to three portions:

(i) an elastic portion ($r > 10\ell$) within which all curves coincide and become a straight line of slope $-1/2$, corresponding to the elastic K field;
(ii) a relatively flat, plastic portion ($r > 0.3\ell$) within which the curves for TNT plasticity and classical plasticity are essentially the same, indicating that the strain gradient effects are not significant above a distance of 0.3ℓ away from the crack tip;
(iii) a portion near the crack tip ($r < 0.3\ell$) within which strain gradient effects are important as evidenced by the wide separation of curves for TNT plasticity and that for classical plasticity; the curve for classical plasticity approaches a straight line with the slope of $-N/(N+1)$, corresponding to the HRR field (Hutchinson, 1968; Rice and Rosengren, 1968) in classical plasticity; the curves for TNT plasticity, however, have much larger slopes with their absolute values exceeding $1/2$, indicating that the crack tip field in TNT plasticity is more singular than not only the HRR field, but also the elastic K field.

It is evident from Fig. 3 that, within this zone of 0.3ℓ near the crack tip, TNT plasticity gives much larger stresses than classical plasticity does. At $r = 0.1\ell$, the effective stress in TNT plasticity is more than twice of

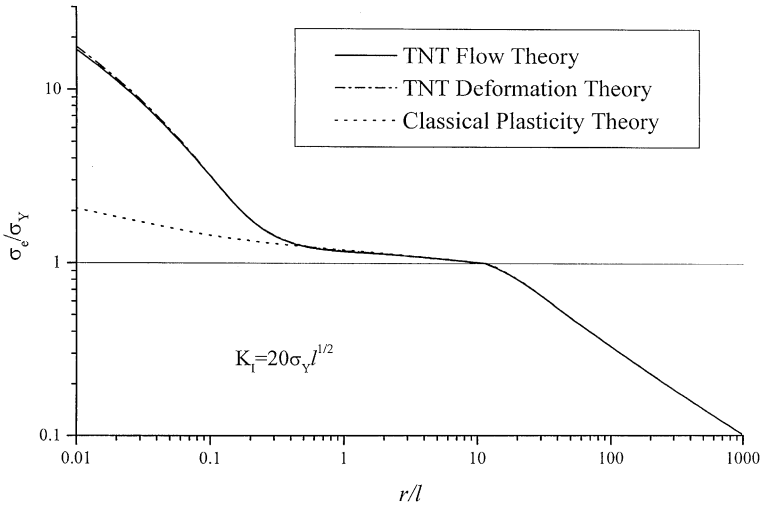

Fig. 3. The effective stress σ_e normalized by the yield stress σ_Y versus the normalized distance ahead of the crack tip, r/ℓ, at polar angle $\theta = 1.014°$, where ℓ is the internal material length in Eq. (3); the plastic work hardening exponent $N = 0.2$, Poisson's ratio $\nu = 0.3$, the ratio of yield stress to Young's modulus $\sigma_Y/E = 0.2\%$, and the remote stress intensity factor $K_I/\sigma_Y\ell^{1/2} = 20$; the results are presented for flow and deformation theories of TNT plasticity, as well as for the classical flow theory of plasticity.

that in classical plasticity. This significant increase in the stress level is clearly due to the strain gradient effects. Since the internal material length ℓ is around 4–5 μm for metallic materials (Fleck et al., 1994; Stolken and Evans, 1998; Gao et al., 1999a), this zone of 0.3ℓ is around 1.5 μm, which is at least one order of magnitude larger than the average dislocation spacing (for a reasonable dislocation density of 10^{14} m^{-2} around the crack tip). The dislocation activities over this scale can still be homogenized and represented by continuum plasticity. Therefore, at a distance to the crack tip over which continuum plasticity still applies, TNT plasticity indeed gives a much higher stress level than classical plasticity does.

It should be pointed out that the size of this zone within which strain gradient effects are significant can be larger than the estimate of 0.3ℓ in Fig. 3. This is because the size of 0.3ℓ is obtained from the comparison of stress distributions in TNT and classical plasticity only ahead of the crack tip, which may not be applicable to other directions (polar angles). Fig. 4 shows the distribution of opening displacement on the crack face, $u_2(\theta = \pi)$, for the flow theories of TNT and classical plasticity. The material parameters and remote stress intensity factor $K_I/\sigma_Y\ell^{1/2} = 20$ are the same as in Fig. 3. The difference between the curves is significant within a distance as large as ℓ to the crack tip, indicating that the strain gradient effects are important within a zone as large as the internal material length ℓ to the crack tip, which is larger than the estimate in Fig. 3.

Fig. 5 shows the distribution of effective stress ahead of the crack tip (polar angle $\theta = 1.014°$) for three remote elastic stress intensity factors, $K_I/\sigma_Y\ell^{1/2} = 5, 10$ and 20. The differences between the flow and deformation theories of TNT plasticity are very small for all three loadings. As the loading increases, the plastic zone size r_p increases rapidly. This is consistent with the estimate from classical plasticity, which predicts $r_p \propto K_I^2$. However, it is observed that the size of the zone within which stresses increase rapidly near the crack tip does not increase much with the loading. This suggests that the size of the dominance zone of the crack tip field in TNT plasticity is relatively insensitive to the applied load, and is essentially on the order of internal material length ℓ.

Fig. 6 shows the distribution of effective stress ahead of the crack tip for the flow theory of TNT plasticity and that of MSG plasticity (Qiu et al., 2001). It is clearly seen that, over the entire range of r from

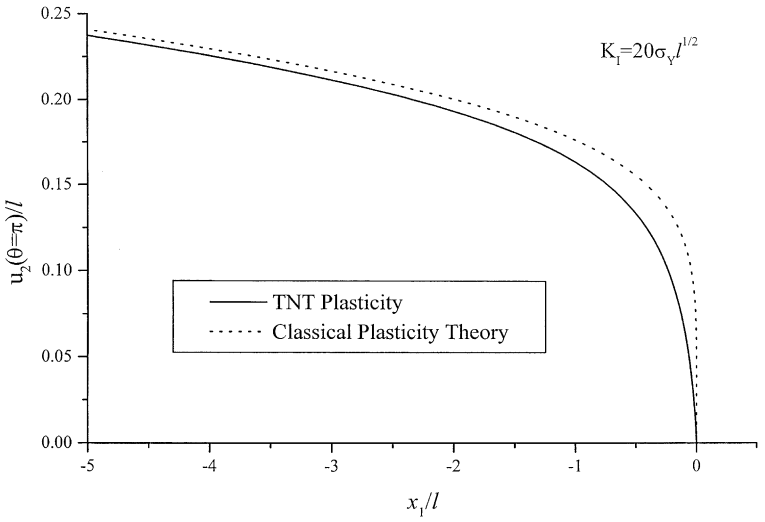

Fig. 4. The crack face opening displacement normalized by the internal material length ℓ for the flow theories of TNT plasticity and classical plasticity. The material and loading parameters are the same as those in Fig. 3.

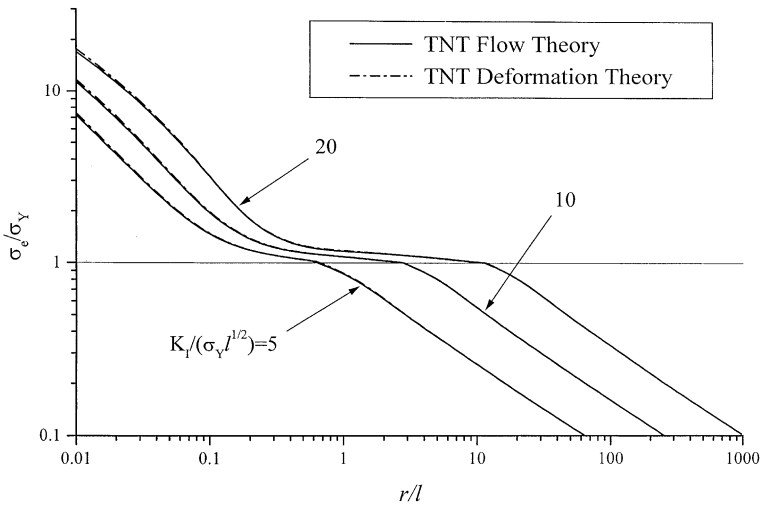

Fig. 5. The distribution of effective stress ahead of the crack tip (at polar angle $\theta = 1.014°$) for both flow and deformation theories of TNT plasticity. The remote stress intensity factor is $K_1/\sigma_Y \ell^{1/2} = 5$, 10 and 20. All normalization and material parameters are the same as those in Fig. 3.

0.01ℓ to $10^3\ell$, TNT plasticity agrees completely with MSG plasticity. This conclusion holds if the higher-order stress traction vanishes on the boundary, as in pure bending, pure torsion, growth of micro-voids, cavitation instabilities (Gao and Huang, 2001), micro-indentation experiments (Section 4), and crack tip field (this section). This once again shows that even though MSG and TNT plasticity are two different mesoscale plasticity theories, they give the same results because both are based on the Taylor dislocation model on the micro-scale.

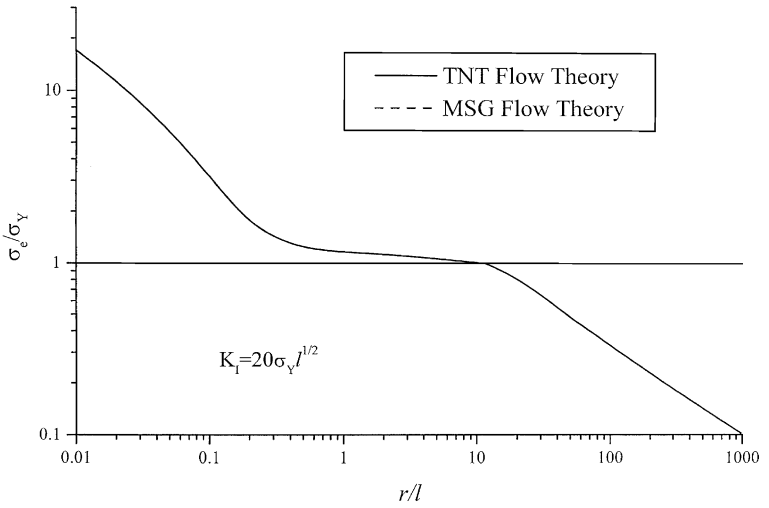

Fig. 6. The effective stress distribution ahead of the crack tip (polar angle $\theta = 1.014°$) for the flow theories of TNT and MSG plasticity. All normalization and material and loading parameters are the same as those in Fig. 3.

6. Summary

The following objectives have been achieved in this paper:

(i) We have developed an effective and robust finite element method for the TNT plasticity (Gao and Huang, 2001).
(ii) We have used the finite element method for TNT plasticity to investigate the micro-indentation experiments. It is established that TNT plasticity agrees well with the micro-indentation hardness data over a wide range of indentation depth, from one-tenth of a micron to several microns.
(iii) The finite element method has also been used to investigate the crack tip field in TNT plasticity. It is established that the stress level in TNT plasticity is significantly larger than that in classical plasticity. The significant stress increase occurs over a distance to the crack tip that is at least one order of magnitude larger than the dislocation spacing such that continuum plasticity still applies. The significant stress increase in TNT plasticity provides an alternative mechanism for cleavage fracture in presence of plastic flow observed in the experiments of Elssner et al. (1994).
(iv) Even though TNT plasticity and MSG plasticity (Gao et al., 1999b; Huang et al., 1999, 2000a,b) belong to different theoretical frameworks, they give the same results in the study of micro-indentation experiments and the crack tip fields. This is because both TNT and MSG plasticity are based on the Taylor dislocation model.

Acknowledgements

YH acknowledges the support from NSF (grant CMS-0084980 and a supplement to grant CMS-9896285 from the NSF International Program). This work was completed while YH was a senior visiting scholar at the Failure Mechanics Lab, Department of Engineering Mechanics, Tsinghua University. HG acknowledges the support from NSF (grant CMS-9979717). The authors acknowledge the support from NSFC.

References

Acharya, A., Bassani, J.L., 2000. Lattice incompatibility and a gradient theory of crystal plasticity. J. Mech. Phys. Solids 48, 1565–1595.

Acharya, A., Beaudoin, A.J., 2000. Grain-size effect in viscoplastic polycrystals at moderate strains. J. Mech. Phys. Solids 48, 2213–2230.

Arsenlis, A., Parks, D.M., 1999. Crystallographic aspects of geometrically-necessary and statistically-stored dislocation density. Acta Mater. 47, 1597–1611.

Ashby, M.F., 1970. The deformation of plastically non-homogeneous alloys. Phil. Mag. 21, 399–424.

Atkinson, M., 1995. Further analysis of the size effect in indentation hardness tests of some metals. J. Mater. Res. 10, 2908–2915.

Bazant, Z.P., 1986. Mechanics of distributed cracking. Appl. Mech. Rev. 26, 675–705.

Bazant, Z.P., Belytschko, T.B., Chang, T.B., 1984. Continuum theory for strain softening. ASCE J. Engng. Mech. 110, 1666–1691.

Bazant, Z.P., Lin, F.B., 1988. Non-local yield limit degradation. Int. J. Numer. Mech. Engng. 26, 1805–1823.

Beaudoin, A.J., Acharya, A., Chen, S.R., Korzekwa, D.A., Stout, M.G., 2000. Consideration of grain-size effect and kinetics in the plastic deformation of metal polycrystals. Acta Mater. 48, 3409–3423.

Begley, M.R., Hutchinson, J.W., 1998. The mechanics of size-dependent indentation. J. Mech. Phys. Solids 46, 2049–2068.

Beltz, G.E., Rice, J.R., Shih, C.F., Xia, L., 1996. A self-consistent method for cleavage in the presence of plastic flow. Acta Mater. 44, 3943–3954.

Chen, E.P., 1999. Non-local effects on dynamic damage accumulation in brittle solids. Int. J. Num. Methods Geomech. 23, 1–22.

Cleveringa, H.H.M., Van Der Giessen, E., Needleman, A., 1997. Comparison of discrete dislocation and continuum plasticity predictions for a composite material. Acta Mater. 45, 3163–3179.

Cleveringa, H.H.M., Van Der Giessen, E., Needleman, A., 1998. Discrete dislocation simulations and size dependent hardening in single slip. J. De Physique. IV 8, 83–92.

Cleveringa, H.H.M., Van Der Giessen, E., Needleman, A., 1999a. Discrete dislocation analysis of bending. Int. J. Plasticity 15, 837–868.

Cleveringa, H.H.M., Van Der Giessen, E., Needleman, A., 1999b. A discrete dislocation analysis of residual stresses in a composite material. Phil. Mag. A 79, 893–920.

Cleveringa, H.H.M., Van Der Giessen, E., Needleman, A., 2000. Discrete dislocation analysis of mode I crack growth. J. Mech. Phys. Solids 48, 1133–1157.

Dai, H., Parks, D.M., 2001. Geometrically necessary dislocation density in continuum crystal plasticity theory and FEM implementation, unpublished.

De Guzman, M.S., Neubauer, G., Flinn, P., Nix, W.D., 1993. The role of indentation depth on the measured hardness of materials. Mater. Res. Symp. Proc. 308, 613–618.

Elssner, G., Korn, D., Ruehle, M., 1994. The influence of interface impurities on fracture energy of UHV diffusion bonded metal-ceramic bicrystals. Scripta Metall. Mater. 31, 1037–1042.

Eringen, A.C., 1981. On nonlocal plasticity. Int. J. Engng. Sci. 19, 1461–1474.

Eringen, A.C., 1983. Theories of nonlocal plasticity. Int. J. Engng. Sci. 21, 741–751.

Fleck, N.A., Hutchinson, J.W., 1993. A phenomenological theory for strain gradient effects in plasticity. J. Mech. Phys. Solids 41, 1825–1857.

Fleck, N.A., Hutchinson, J.W., 1997. Strain gradient plasticity. In: Hutchinson, J.W., Wu, T.Y. (Eds.), Adv. Appl. Mech., vol. 33. Academic Press, New York, pp. 295–361.

Fleck, N.A., Muller, G.M., Ashby, M.F., Hutchinson, J.W., 1994. Strain gradient plasticity: theory and experiments. Acta Metall. Mater. 42, 475–487.

Gao, H., Huang, Y., 2001. Taylor-based nonlocal theory of plasticity. Int. J. Solids Struct. 38, 2615–2637.

Gao, H., Huang, Y., Nix, W.D., 1999a. Modeling plasticity at the micrometer scale. Naturwissenschaftler 86, 507–515.

Gao, H., Huang, Y., Nix, W.D., Hutchinson, J.W., 1999b. Mechanism-based strain gradient plasticity – I. Theory. J. Mech. Phys. Solids 47, 1239–1263.

Gurtin, M.E., 2000. On the plasticity of single crystals: free energy, microforces, plastic-strain gradients. J. Mech. Phys. Solids 48, 989–1036.

Huang, Y., Gao, H., Hwang, K.C., 1999. Strain-gradient plasticity at the micron scale. In: Ellyin, F., Provan, J.W. (Eds.), Progress in Mechanical Behavior of Materials, vol. III, pp. 1051–1056.

Huang, Y., Gao, H., Nix, W.D., Hutchinson, J.W., 2000a. Mechanism-based strain gradient plasticity – II. Analysis. J. Mech. Phys. Solids 48, 99–128.

Huang, Y., Xue, Z., Gao, H., Nix, W.D., Xia, Z.C., 2000b. A study of micro-indentation hardness tests by mechanism-based strain gradient plasticity. J. Mater. Res. 15, 1786–1796.

Hutchinson, J.W., 1997. Linking scales in mechanics. In: Karihaloo, B.L., Mai, Y.W., Ripley, M.I., Ritchie, R.O. (Eds.), Adv. Fract. Res., Pergamon Press, Oxford, pp. 1–14.

Hutchinson, J.W., 1968. Singular behavior at the end of a tensile crack in a hardening material. J. Mech. Phys. Solids 16, 13–31.
Lloyd, D.J., 1994. Particle reinforced aluminum and magnesium matrix composites. Int. Mater. Rev. 39, 1–23.
Ma, Q., Clarke, D.R., 1995. Size dependent hardness of silver single crystals. J. Mater. Res. 10, 853–863.
McElhaney, K.W., Vlassak, J.J., Nix, W.D., 1998. Determination of indenter tip geometry and indentation contact area for depth-sensing indentation experiments. J. Mat. Res. 13, 1300–1306.
Needleman, A., 2000. Computational mechanics at the mesoscale. Acta Mater. 48, 105–124.
Nix, W.D., 1989. Mechanical properties of thin films. Met. Trans. A 20A, 2217–2245.
Nix, W.D., 1997. Elastic and plastic properties of thin films on substrates: nanoindentation techniques. Mat. Sci. Engng. A A234–236, 37–44.
Nix, W.D., Gao, H., 1998. Indentation size effects in crystalline materials: a law for strain gradient plasticity. J. Mech. Phys. Solids 46, 411–425.
Nix, W.D., Gibeling, J.C., 1985. Mechanism of time-dependent flow and fracture of metals. Metals/Materials Technology Series 8313–004. ASM, Metals Park, OH.
Pijaudier-Cabot, G., Bazant, Z.P., 1987. Nonlocal damage theory. ASCE J. Engng. Mech. 10, 1512–1533.
Poole, W.J., Ashby, M.F., Fleck, N.A., 1996. Micro-hardness of annealed and work-hardened copper polycrystals. Scripta Metall. Mater. 34, 559–564.
Qiu, X., Huang, Y., Gao, H., Zhuang, Z., Hwang, K.C., 2001. The flow theory of mechanism-based strain gradient plasticity, submitted for publication.
Rice, J.R., Rosengren, G.F., 1968. Plane strain deformation near a crack tip in a power law hardening material. J. Mech. Phys. Solids 16, 1–12.
Shu, J.Y., Fleck, N.A., 1998. The prediction of a size effect in micro-indentation. Int. J. Solids Struct. 35, 1363–1383.
Shu, J.Y., Fleck, N.A., 1999. Strain gradient crystal plasticity: size-dependent deformation of bicrystals. J. Mech. Phys. Solids 47, 292–324.
Shu, J.Y., Fleck, N.A., Van Der Giessen, E., Needleman, A., 2001. Boundary layers in constrained plastic flow: comparison of nonlocal and discrete dislocation plasticity. J. Mech. Phys. Solids, in press.
Stelmashenko, N.A., Walls, M.G., Brown, L.M., Milman, Y.V., 1993. Microindentation on W and Mo oriented single crystals: an STM study. Acta Metall. Mater. 41, 2855–2865.
Stolken, J.S., Evans, A.G., 1998. A microbend test method for measuring the plasticity length scale. Acta Mater. 46, 5109–5115.
Stromberg, L., Ristinmaa, M., 1996. FE-formulation of a nonlocal plasticity theory. Comp. Met. Appl. Mech. Engng. 136, 127–144.
Suo, Z., Shih, C.F., Varias, A.G., 1993. A theory for cleavage cracking in the presence of plastic flow. Acta Metall. Mater. 41, 1551–1557.
Suresh, S., Nieh, T.G., Choi, B.W., 2000. Nano-indentation of copper thin films on silicon substrates. Scripta Materialia 41, 951–957.
Wei, Y., Hutchinson, J.W., 1999. Models of interface separation accompanied by plastic dissipation at multiple scales. Int. J. Fract. 95, 1–17.